


Characterization of polarization gating parameters for attosecond pulse generation using an imaging polarimeter

Tomoya Okino * and Katsumi Midorikawa *Attosecond Science Research Team, RIKEN Center for Advanced Photonics, 2-1 Hirosawa, Wako-shi, Saitama 351-0198, Japan*

(Received 10 April 2020; accepted 30 July 2020; published 21 August 2020)

Isolated attosecond pulses can be generated by the polarization gating method, for which the gating time window and the polarization direction are key parameters. In this work, we propose methods to characterize these parameters with an imaging polarimeter based on the division of the focal plane in a single-shot manner. The gating time window and the polarization direction can be characterized using the degree of linear polarization and the angle of linear polarization, respectively. Spatially resolved evaluation of gating parameters is important for generating high-intensity isolated attosecond pulses. The robust generation of isolated attosecond pulses by evaluating the gating parameters with the proposed method will enable us to perform the attosecond-pump and attosecond-probe of electron dynamics in atoms and molecules.

DOI: [10.1103/PhysRevA.102.023116](https://doi.org/10.1103/PhysRevA.102.023116)

I. INTRODUCTION

Observing the motion of electrons is crucial for understanding the fundamental processes in atoms and molecules [1]. Manipulating the electron distribution in a molecule will offer a new method for controlling chemical reactions [2] and developing new materials [3]. Because the intrinsic timescale of electron motion is in attoseconds, pump-probe measurements with attosecond temporal resolution should be implemented.

Attosecond optical pulses can be generated by a coherent light conversion process known as high-order harmonic generation (HHG) [4–7]. In the HHG process, attosecond pulses are generated every half optical cycle of the central frequency of the driving laser where the phase among the harmonics is locked. An isolated attosecond pulse (IAP) with only one attosecond pulse in the envelope can be generated using a carrier-envelope phase (CEP) stabilized few-cycle pulse as a driving laser pulse, where electron recollision in the HHG can be confined within one-half of the optical cycle by suppressing the recollision probability in adjacent half-cycles.

To moderate the demand of the driving laser and generate the IAP with a high pulse contrast, several gating methods have been proposed and demonstrated, such as polarization gating (PG) [8–11], two-color gating (TCG) [12], and double optical gating (DOG) [13]. The gating methods are mainly based on the intrinsic nature of the HHG process, namely that the process is sensitive to (i) the peak field intensity and (ii) the ellipticity of the driving laser pulse.

In the PG, counterrotating circularly polarized pulses are temporally overlapped with an appropriate delay to generate ultrashort pulses with quasilinear polarization only in the subcycle time window. While PG is efficient for generating the IAP with high pulse contrast, it is sensitive to the gate width determined by the delay between the counterrotating

circularly polarized pulses [14]. In the HHG process, the polarization angle or the polarization direction of the high harmonics coincides with the polarization direction of the driving laser. Therefore, the polarization direction of the quasilinearly polarized pulse in the gating time window reflects the polarization direction of the IAP.

In the pump-probe measurement using the IAP, the polarization direction of the IAP should be determined by the downstream experimental setup, because there are no efficient optics in the XUV wavelength region for manipulating the polarization of the IAP. In the momentum imaging of ions and photoelectrons using a velocity map imaging spectrometer [15], the electric field requires cylindrical symmetry to retrieve the three-dimensional momentum images based on the Abel inversion of the experimental raw data. Moreover, the polarization direction of the IAP should be stable in the designed direction in the attosecond transient absorption spectroscopy for atoms [16] and molecules [17] because the angle between the near infrared pump pulse and the IAP probe pulse determines the transition probability between the electronic states and, therefore, fluctuations of the polarization direction of the IAP will be problematic for quantitative analysis of pump-probe measurements using the IAP.

In the PG method, the delay determining the polarization direction in the gating time window is generated with a birefringent crystal plate. Because the retardation of the birefringent plate is inversely proportional to the wavelength of the incident light, the spectrum of the incident few-cycle pulses affects the amount of retardation. It should be noted that, when the central wavelength of the incident pulse changes from the default value, the polarization direction of the IAP changes due to the variation of the gate width, which is problematic for pump-probe measurements requiring long-term data acquisition.

In studies to date, it is typically assumed that the spectrum of the driving laser pulse is spatially uniform, but this is not obvious for broadband light pulses. Broadband light with a

*tomoya.okino@riken.jp

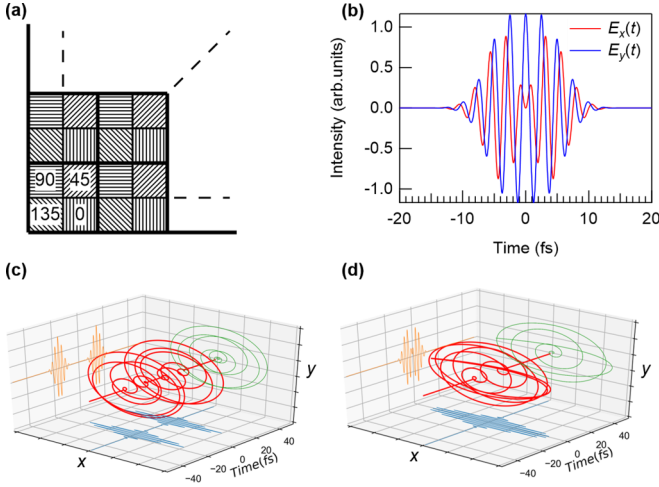


FIG. 1. (a) Schematic drawing of the imaging polarimeter. (b) Electric fields $\{E_x(t), E_y(t)\}$ in the polarization gating (central wavelength $\lambda_c = 750$ nm, pulse duration $\tau_p = 5$ fs, delay $T_d = 6.25$ fs). (c) Counterrotating circular polarized pulses without temporal overlap. (d) Counterrotating circular polarized pulse with adequate temporal overlap.

spectral bandwidth of a few optical cycles can be generated with self-phase modulation processes in a hollow fiber [18], in filamentation [19] or in multiple-thin-plate compression [20]. In these schemes, it is still challenging to generate a uniform spectrum over the entire beam profile [21,22].

In this work, we propose a simple method for the spatially resolved characterization of the gate width and the polarization direction in gating methods for generating IAPs using an imaging polarimeter based on the division of the focal plane [23]. The gate width and the polarization direction are characterized by the degree of linear polarization (DoLP) and the angle of linear polarization (AoLP), respectively. The method in this work is only applicable to the case when the high-order harmonics are generated with an isotropic medium such as an atom with a spherically symmetric ground state. However, the spatially resolved measurement can be used for evaluating the input beam uniformity even when the high-order harmonics are generated with a nonisotropic medium. If the input beam is uniform, both the AoLP and the DoLP should be the same values reflecting the same gating parameters.

II. PRINCIPLE

A. Polarization gating

A schematic of the imaging polarimeter is shown in Fig. 1(a). It features four-directional wire grid polarizers on a complementary metal oxide semiconductor (CMOS) sensor and can record the linear Stokes parameters (S_0, S_1, S_2) from the intensity of 2×2 pixels ($I_0, I_{45}, I_{90}, I_{135}$). The two parameters, DoLP and AoLP, that characterize the gating parameters in the PG method are evaluated by

$$\text{DoLP} = \frac{\sqrt{S_1^2 + S_2^2}}{S_0}, \quad (1)$$

$$\text{AoLP} = \frac{1}{2} \tan^{-1} \left(\frac{S_2}{S_1} \right), \quad (2)$$

where $S_0 = I_0 + I_{90}$, $S_1 = I_0 - I_{90}$, and $S_2 = I_{45} - I_{135}$.

The electric fields $\{E_x^{\text{PG}}(t), E_y^{\text{PG}}(t)\}$ in PG are expressed by

$$E_x^{\text{PG}}(t) = A_+ \cos[\omega(t + T_d/2) + \phi_{\text{CE}}] + A_- \cos[\omega(t - T_d/2) + \phi_{\text{CE}}], \quad (3)$$

$$E_y^{\text{PG}}(t) = A_+ \sin[\omega(t + T_d/2) + \phi_{\text{CE}}] - A_- \sin[\omega(t - T_d/2) + \phi_{\text{CE}}], \quad (4)$$

where T_d is the delay between the counterrotating circularly polarized pulses, ω is the central frequency, and ϕ_{CE} is the CEP of the fundamental pulse. A_+ and A_- are envelope functions of the electric field of counterrotating circularly polarized pulses.

The delay T_d generated with the birefringent plate is given by $T_d = (\frac{1}{v_e} - \frac{1}{v_o})L$, where L is the thickness of the birefringent plate and v_e and v_o are the velocities of the extraordinary and ordinary beams. Note that the nominal polarization direction of an IAP is determined by T_d . T_d should be an integer multiple of the half optical cycle of the fundamental pulse $T_d = 1/2nT_0$ ($n = 1, 2, \dots$) (T_0 , optical cycle of the fundamental pulse) based on the layout of the downstream experimental setup. For example, in the case of the electric fields depicted in Fig. 1(b) (central wavelength of $\lambda_c = 750$ nm, $\tau_p = 5$ fs, and $T_d = 6.25$ fs with a Gaussian temporal profile), the IAP is polarized in the y direction.

The gate width τ_g describing a duration with a quasilinear polarization in the PG method can be evaluated by [11]

$$\tau_g = \frac{\varepsilon_{\text{thr}} \tau_p^2}{\ln(2)T_d}, \quad (5)$$

where ε_{thr} is the threshold ellipticity of the driving laser pulse ($\varepsilon_{\text{thr}} = 0.2$ for 800 nm [24]). The general criterion for obtaining the IAP in the PG method is that τ_g is smaller than half the optical cycle of the fundamental pulse $T_0/2$.

The Stokes parameters S_0, S_1 , and S_2 can be expressed as

$$\begin{pmatrix} S_0 \\ S_1 \\ S_2 \end{pmatrix} = \begin{pmatrix} \int (A_+^2 + A_-^2) dt \\ \cos \omega T_d \int 2A_+ A_- dt \\ \sin \omega T_d \int 2A_+ A_- dt \end{pmatrix}. \quad (6)$$

Even though the Stokes parameters are obtained by the time-integrated four-directional signals ($I_0, I_{45}, I_{90}, I_{135}$), S_1 and S_2 can carry information on the quasilinearly polarized gate time window because the circular polarized components of the electric field in the PG method are canceled. The DoLP can be regarded as the intensity fraction of quasilinearly polarized components. In fact, when $T_d = 0$ (perfect temporal overlap, linear polarization in the x direction) or $T_d \gg \tau_p$ (no temporal overlap), $\text{DoLP} = 1$ or 0, respectively. In the PG method, the DoLP satisfies $0 < \text{DoLP} < 1$ as an intermediate of two extreme cases. On the other hand, the AoLP is identical to the polarization direction at $t = 0$ because the ratio of the electric field between the x direction and the y direction at $t = 0$ is $E_y^{\text{PG}}(0)/E_x^{\text{PG}}(0) = \tan(\omega T_d/2) = \tan(\text{AoLP})$. It should be noted that the formulas for S_0, S_1 , and S_2 shown in Eq. (6)

are valid irrespective of the pulse envelope shape. The DoLP and the AoLP obtained from the four-directional intensities accompanying the time-integration of photon signals can be used to evaluate the degree of linear polarization and the polarization direction in the gate time window.

When the pulse envelope is Gaussian in Eqs. (3) and (4), S_0 , S_1 , and S_2 can be expressed as

$$\begin{pmatrix} S_0 \\ S_1 \\ S_2 \end{pmatrix} = \begin{pmatrix} \sqrt{\frac{\pi}{\ln 2}} \tau_p \\ 2^{-(T_d/\tau_p)^2} \cos \omega T_d S_0 \\ 2^{-(T_d/\tau_p)^2} \sin \omega T_d S_0 \end{pmatrix}. \quad (7)$$

The DoLP and the AoLP can be simplified as

$$\text{DoLP} = 2^{-(T_d/\tau_p)^2}, \quad (8)$$

$$\text{AoLP} = \frac{1}{2} \omega T_d, \quad (9)$$

where the AoLP should be in the range $|\text{AoLP}| \leq \pi/2$. When the AoLP is 0 and $\pi/2$, the emission polarization of the IAP is in the x and y directions, respectively. From Eqs. (5) and (8), the DoLP_{max} satisfying $\tau_g = T_0/2$ can be evaluated by

$$\text{DoLP}_{\text{max}} = \exp \left[-\frac{1}{\ln 2} \left(\frac{2\varepsilon_{\text{thr}} \tau_p}{T_0} \right)^2 \right]. \quad (10)$$

The polarization direction of the IAP at DoLP = DoLP_{max} does not always exhibit the designed angle based on the downstream experimental setup, and T_d should be designed for the default polarization direction of the IAP by compromising the DoLP or the intensity in the gate time window. As the number of optical cycles τ_p/T_0 or ε_{thr} decreases, the DoLP_{max} increases, suggesting that the intensity contributing to the generation of IAPs increases. For example, when there is no temporal overlap between the counterrotating circularly polarized pulses as shown in Fig. 1(c), the DoLP is zero and the AoLP is unspecified. On the other hand, as the temporal overlap of two counterrotating pulses increases, the DoLP increases monotonically. For the electric fields shown in Fig. 1(d), DoLP = 0.339 and AoLP = 90°.

It should be noted that the AoLP is proportional to ω and T_d (or L), and changes in these should be kept small to maintain the same polarization direction of the IAP during the data acquisition. T_d cannot be determined uniquely only from the AoLP. With a combination of the AoLP and the DoLP, T_d can be precisely measured and τ_g can be retrieved.

B. Two-color gating

The TCG method is one of the simplest gating methods for generating an IAP, in which the intensity at $\pm T_0/2$ is suppressed by superposing another linearly polarized pulse with a different central frequency [12]. Typically, a weak second-order harmonic field is superposed to break the symmetry of the electric field to improve the intensity contrast between the highest peak at $t = 0$ and the adjacent peaks at $t = \pm T_0/2$ of the attosecond burst. In the following, we consider only a specific TCG case where the second-order harmonic field is superposed on the fundamental field. In TCG, the synthesized electric field is linearly polarized and the emission polarization of the IAP is the same as the polarization angle

of the driving laser. The intensity ratio of the two frequency components, the pulse durations of the two-color components, and the relative phase between two frequency components are key parameters to be optimized in TCG. However, it is not trivial to assume that the two-color parameters, such as the amplitude ratio and the relative phase $\phi_{\omega,2\omega}$ between the two-color pulses, are spatially uniform.

Using a full-Stokes imaging polarimeter [25], the relative phase $\phi_{\omega,2\omega}$ can be evaluated as a snapshot. The electric field in TCG, $E_x(t)^{\text{TCG}}$, can be expressed as

$$E_x(t)^{\text{TCG}} = A \cos(\omega t + \phi_{\text{CE}}) + pB \cos(2\omega t + 2\phi_{\text{CE}} + \phi_{\omega,2\omega}). \quad (11)$$

The auxiliary second-order harmonic of the fundamental light generated with Type-I phase matching in the y direction is expressed as

$$E_y(t)^{\text{AUX}} = qC \cos(2\omega t + 2\phi_{\text{CE}}). \quad (12)$$

p and q are the amplitude ratio of the second-order harmonic in TCG and the second-order harmonic in the auxiliary field with respect to the fundamental pulse. The envelope functions are given by $A = \exp[-2 \ln 2 (t/\tau_{1p})^2]$, $B = \exp[-2 \ln 2 (t/\tau_{2p})^2]$, and $C = \exp[-2 \ln 2 (t/\tau_{1p'})^2]$, where τ_{1p} , τ_{2p} , and $\tau_{1p'}$ are the pulse duration of the fundamental pulse, the second-order harmonic in TCG, and the second-order harmonic in the auxiliary field, respectively. The relative phase $\phi_{\omega,2\omega}$ is extracted using $\{E_x(t)^{\text{TCG}}, E_y(t)^{\text{AUX}}\}$ by recording the Stokes parameters.

The Stokes parameters can be described by

$$\begin{pmatrix} S_0 \\ S_1 \\ S_2 \\ S_3 \end{pmatrix} = \frac{1}{4} \begin{pmatrix} 1 + bp^2 + cq^2 \\ 1 + bp^2 - cq^2 \\ \frac{bc}{\sqrt{2(b^2+c^2)}} pq \cos \phi_{\omega,2\omega} \\ \frac{bc}{\sqrt{2(b^2+c^2)}} pq \sin \phi_{\omega,2\omega} \end{pmatrix} A_0, \quad (13)$$

where b and c are the ratios of the pulse durations $b = \tau_{2p}/\tau_{1p}$ and $c = \tau_{1p'}/\tau_{1p}$, and $A_0 = \sqrt{\pi/\ln 2} \tau_{1p}$. From S_2 and S_3 using the full-Stokes imaging polarimeter, the relative phase $\phi_{\omega,2\omega}$ can be retrieved as a snapshot. To completely characterize the TCG parameters, the spatial intensity ratio of the two-color pulses $I_{2\omega}/I_\omega = bp^2$ should be determined. When $b = c$ or $\tau_{2p} = \tau_{1p'}$ is satisfied, bp^2 and bq^2 can be determined from the Stokes parameters in Eq. (13) in addition to the relative phase $\phi_{\omega,2\omega}$.

C. Double optical gating

DOG combines the TCG and PG methods [13,26,27]. In DOG, a shorter IAP can be generated with a relatively long driving pulse compared with the PG method. The electric fields in DOG, $\{E_x^{\text{DOG}}(t), E_y^{\text{DOG}}(t)\}$, are expressed as

$$\begin{aligned} E_x^{\text{DOG}}(t) &= A_+ \cos[\omega(t + T_d/2) + \phi_{\text{CE}}] \\ &\quad + A_- \cos[\omega(t - T_d/2) + \phi_{\text{CE}}] \\ &\quad + aB \cos(2\omega t + 2\phi_{\text{CE}} + \phi), \end{aligned} \quad (14)$$

$$\begin{aligned} E_y^{\text{DOG}}(t) &= A_+ \sin[\omega(t + T_d/2) + \phi_{\text{CE}}] \\ &\quad - A_- \sin[\omega(t - T_d/2) + \phi_{\text{CE}}], \end{aligned} \quad (15)$$

where a is the amplitude ratio between the fundamental pulse and the second-order harmonic, ϕ is the relative phase between the fundamental pulse and the second-order harmonic fields, and B is the envelope of the second-order harmonic.

In the case when the pulse envelopes for the fundamental pulse and second-order harmonic are Gaussian, the DoLP and the AoLP can be expressed as

$$\text{DoLP} = D_0 \frac{\sqrt{\left(1 + \frac{a^2b}{4D_0}\right)^2 - \frac{a^2b}{D_0} \sin^2\left(\frac{\omega T_d}{2}\right)}}{1 + \frac{a^2b}{4}}, \quad (16)$$

$$\text{AoLP} = \frac{1}{2} \tan^{-1}\left(\frac{\sin \omega T_d}{\cos \omega T_d + \frac{a^2b}{4D_0}}\right), \quad (17)$$

where D_0 is the DoLP in PG as shown in Eq. (8). It should be noted that identical DoLP and AoLP values are obtained irrespective of ϕ and ϕ_{CE} because the ϕ and ϕ_{CE} dependencies are canceled in the time integration. More precisely, the time-integral of the product of the different frequency components such as $\cos(\omega t + \theta_1) \cos(2\omega t + \theta_2)$, where θ_1 and θ_2 are phase components of the fundamental pulse and the second-order harmonic, are zero.

When the intensity of the second-order harmonic is much smaller than that of the fundamental pulse, $a^2b \ll 1$ (or $I_{2\omega}/I_\omega \ll 1$) is fulfilled. In this case, Eq. (16) can be simplified as

$$\text{DoLP} = D_0 \frac{\sqrt{1 + \frac{a^2b}{2D_0} \cos \omega T_d}}{1 + \frac{a^2b}{4}}. \quad (18)$$

As shown in Eq. (17), T_d satisfying $\text{AoLP} = 0$ does not depend on the parameters of the second-order harmonic because the optimum delay can be found when $\sin \omega T_d = 0$ is satisfied. When the term $a^2b/4D_0$ in Eq. (17) is larger than 1, $\text{AoLP} = \pm 90^\circ$ cannot be realized. This corresponds to the case when the second-order harmonic intensity is strong and/or T_d is too large, leading to poor temporal overlap between the counterrotating circularly polarized pulses. In these cases, the emission polarization direction of the IAP is dominantly determined by the polarization direction of the second-order harmonic. Therefore, the AoLP is also a good measure in DOG.

III. RESULTS AND DISCUSSION

A. Polarization gating

1. Gaussian pulse shape

Figure 2(a) shows τ_g and the DoLP as functions of L and T_d between counterrotating circularly polarized few-cycle pulses ($\lambda = 750$ nm, $\tau_p = 5$ fs). Quartz is selected as a birefringent crystal and the refractive indices for the ordinary and extraordinary beams are calculated from the Sellmeier equation [28]. There is a one-to-one correspondence between the gate width and the DoLP as described in Eq. (5). If L is larger than $182 \mu\text{m}$ where $\text{DoLP}_{\text{max}} = 0.395$, τ_g can be shorter than $T_0/2$. However, the actual adequate τ_g and T_d are determined by the designed polarization direction in the gating time window.

In Fig. 2(b), the AoLP and the DoLP are plotted as functions of L and T_d . The polarization angle of the laser pulse in the gate window corresponding to the emission polarization

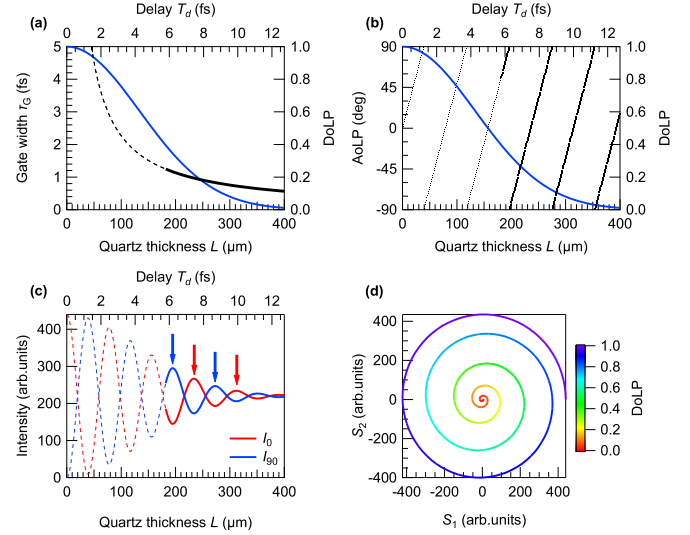


FIG. 2. T_d and L dependence of (a) τ_g (black) and DoLP (blue/gray), (b) AoLP (black) and DoLP (blue/gray), and (c) intensity I_0 (red) and I_{90} (blue) in the imaging polarimeter. The red and blue arrows show the AoLP of 0° and 90° , respectively. The solid curves in panels (a)–(c) show T_d and L satisfying $\tau_g \leq T_0/2$. (d) S_1 - S_2 diagram. The color of the curve corresponds to the DoLP.

of the IAP changes linearly as a function of T_d . It should be noted that T_d cannot be determined uniquely only from the AoLP, because there are several delays with the same AoLP. However, the gate width and the emission polarization can be quantitatively characterized by a combination of the AoLP and the DoLP.

The intensities I_0 and I_{90} are plotted as functions of T_d in Fig. 2(c). As T_d increases, I_0 and I_{90} approach 0.5 because I_0 and I_{90} are the same when there is no temporal overlap between two circularly polarized pulses. It should be noted that I_0 and I_{90} correspond to the field autocorrelation. When $T_d = 6.25$ fs, the emission polarization direction is the y direction because $\text{AoLP} = 90^\circ$ and I_{90} and I_0 are at a local maximum and a local minimum. On the other hand, when $T_d = 7.50$ fs, the emission polarization direction is the x direction because $\text{AoLP} = 0^\circ$ and I_0 and I_{90} are at a local maximum and a local minimum. Because the DoLP at $T_d = 6.25$ fs is larger than that at $T_d = 7.50$ fs, $T_d = 6.25$ fs is optimum for generating the strongest IAP whereas DoLP at $T_d = 7.50$ fs is better for generating the IAP with the high contrast. The Stokes parameter S_1 - S_2 diagram is shown in Fig. 2(d). The half angle corresponds to AoLP and the radius corresponds to the DoLP. Because both the DoLP and the AoLP are normalized parameters, the values are insensitive to the shot-by-shot intensity instability of the light pulses.

Typically, the spectrum of a few-cycle pulse is far from a Gaussian spectrum and the central frequency can be changed by varying the laser parameters. For example, when $\lambda_c = 750$ nm, the AoLP is 0° at $L = 235.8 \mu\text{m}$. With the same quartz thickness, the AoLP is 8.2° at $\lambda_c = 740$ nm and -7.9° at $\lambda_c = 760$ nm. Because the variation of the AoLP is proportional to T_d , it is important to fix the central wavelength, particularly for a large T_d or small τ_g . On the other hand, when there is uncertainty in the thickness of the quartz plate,

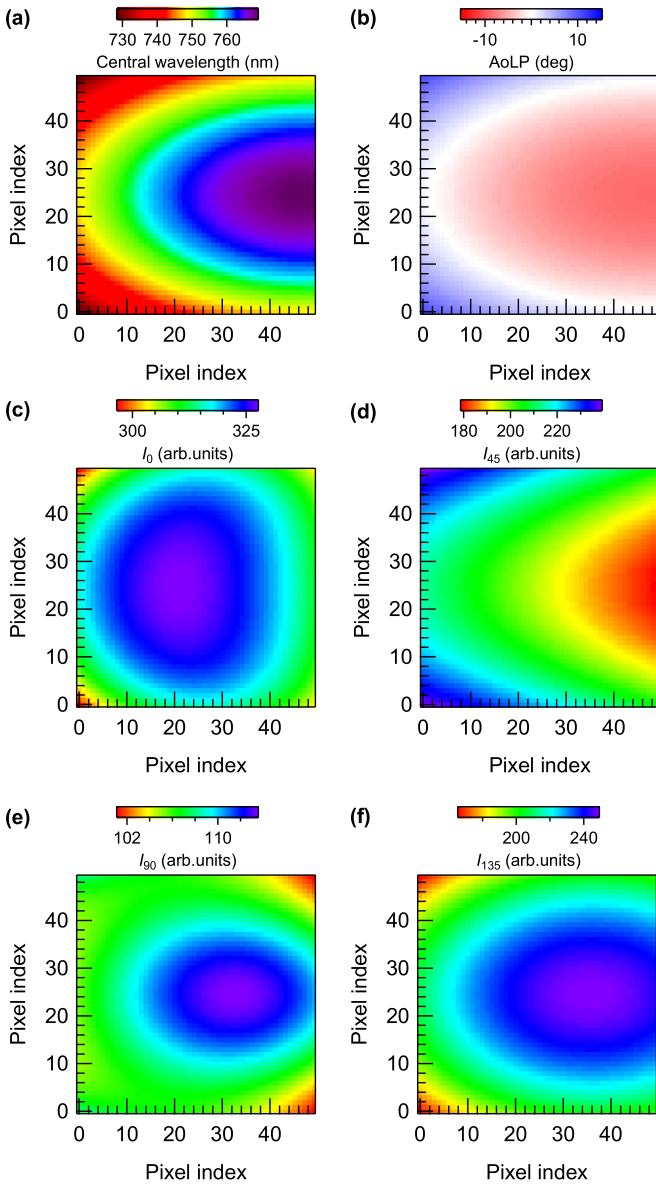


FIG. 3. Spatially resolved simulation. (a) Central wavelength, (b) AoLP, (c) I_0 , (d) I_{45} , (e) I_{90} , and (f) I_{135} .

$\Delta L = 5 \mu\text{m}$, in the fabrication process, the AoLP changes $\pm 11.5^\circ$ at $\lambda_c = 750 \text{ nm}$. Also, when the incident angle to the quartz plate changes by 1° , the AoLP changes by 4.1° . Therefore, the evaluation setup for the gating parameters in the daily operation is crucial for generating a reproducible IAP in the PG method.

2. Gaussian pulse shape with spatially uniform central wavelength

When the spatial distribution of the central wavelength of the electric fields given by Fig. 3(a) is assumed, the AoLP corresponding to the polarization direction of the IAP is simulated as Fig. 3(b), where the pulse durations τ_p and T_d are set to 5 fs. The spatial dependencies of the four-directional intensities with the imaging polarimeter are shown in Figs. 3(c)–3(f) assuming a Gaussian spatial beam profile. Based on these four images, the AoLP map in Fig. 3(b) can be calculated. Here, the DoLP is 0.5 and is independent of

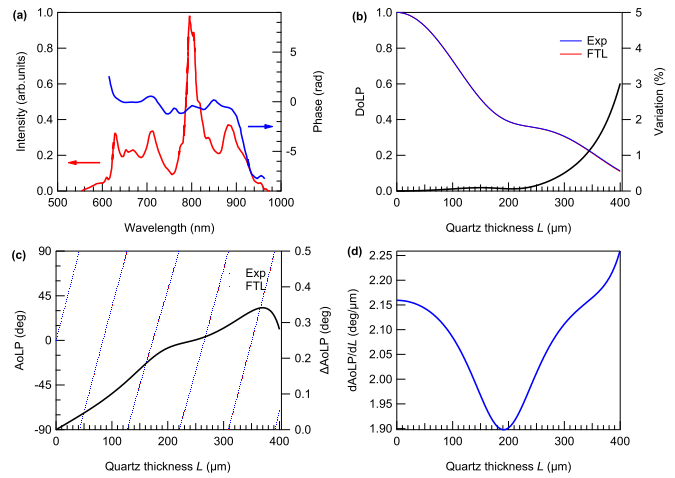


FIG. 4. (a) Spectrum and spectral phase of few-cycle pulses in Ref. [19]. (b) Quartz thickness L dependence of the DoLP with the experimental phase (blue) and the Fourier-transform limited phase (red). The variation is defined as $(\text{DoLP}^{\text{Exp}} - \text{DoLP}^{\text{FTL}})/\text{DoLP}^{\text{FTL}} \times 100$. (c) Quartz thickness L dependence of the AoLP with the experimental phase (blue) and the Fourier-transform limited phase (red) and ΔAoLP ($\Delta\text{AoLP} = \text{AoLP}^{\text{Exp}} - \text{AoLP}^{\text{FTL}}$). (d) Quartz thickness L dependence of $d\text{AoLP}/dL$.

the spatial beam profile and the central wavelength since the DoLP only depends on τ_p and T_d as shown in Eq. (8). On the other hand, the AoLP changes significantly depending on the central wavelength. Due to the multiplex detection of the four-directional intensities, the spatial dependence of AoLP can be precisely obtained. When birefringent quartz wedge plates are used to control T_d , the polarization direction of the IAP can be adjusted or optimized from the AoLP map.

It should be noted that when the input pulse duration is doubled ($\tau_p = 10 \text{ fs}$), the quartz thickness should be four times larger to maintain the same gate width. In this case, the DoLP will be significantly lower ($\text{DoLP}_{\text{max}} = 0.0249$ for $\tau_p = 10 \text{ fs}$ and 0.397 for $\tau_p = 5 \text{ fs}$).

3. Non-Gaussian pulse shape

When the experimentally reported few-cycle pulses [19] shown in Fig. 4(a) are utilized as a driving laser pulse in the PG method, the quartz thickness dependence of the DoLP and the AoLP can be calculated as shown in Figs. 4(b) and 4(c), respectively. In Fig. 4(b), the quartz thickness dependence of the DoLP is calculated using both the experimentally measured spectral phase and the flat phase, giving to the Fourier-transform limited pulse. In both cases, the DoLP changes monotonically as a function of L even though there are some inflection points originating from the pedestal pulses. Although the gate width cannot be exactly retrieved from the DoLP when the spectrum is far from the Gaussian distribution, there is still a one-to-one correspondence between the gate width and the DoLP. The variation, defined as $(\text{DoLP}^{\text{Exp}} - \text{DoLP}^{\text{FTL}})/\text{DoLP}^{\text{FTL}} \times 100$, is less than 3% for a large delay or $L = 400 \mu\text{m}$.

The quartz thickness dependence of the AoLP is calculated in Fig. 4(c). Both curves are almost identical and the difference of the AoLP, $\Delta\text{AoLP} = \text{AoLP}^{\text{Exp}} - \text{AoLP}^{\text{FTL}}$,

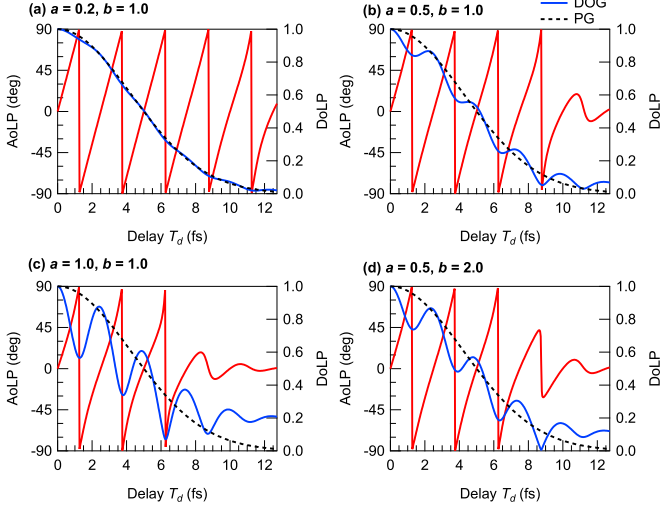


FIG. 5. Delay T_d dependence of the AoLP (red) and the DoLP (blue) in the DOG method. (a) $(a, b) = (0.2, 1.0)$, (b) $(a, b) = (0.5, 1.0)$, (c) $(a, b) = (1.0, 1.0)$, and (d) $(a, b) = (0.5, 2.0)$. The black dotted curves correspond to the DoLP in the PG method. In the simulation, $\tau_{1p} = 5$ fs with $\lambda_c = 750$ nm is assumed.

is less than 0.4° for the entire region of the quartz thickness. In the case of driving laser pulses with a Gaussian temporal profile, the AoLP is linearly proportional to the quartz thickness. However, when the temporal profile is not Gaussian, the AoLP is not perfectly linearly proportional to the quartz thickness and the derivative of the AoLP by L , $d\text{AoLP}/dL$, as shown in Fig. 4(d). The variation is ascribed to the change in the carrier frequency in the gate time window. This result suggests that the thickness of the birefringent plate should be carefully designed for the few-cycle pulse with a structured spectrum. When the delay is small, the contribution of the pedestal component is negligibly small. In other words, the overlapped time window originates from the central part of the pulse. Therefore, the AoLP is a good measure for determining the adequate quartz thickness for the designed polarization direction.

These results suggest that the proposed method is also applicable to few-cycle pulses with non-Gaussian spectra and some uncompressed phases.

B. Double optical gating

In Fig. 5, the AoLP and the DoLP in DOG, simulated for $\tau_{1p} = 5$ fs with $\lambda_c = 750$ nm, are plotted as functions of T_d . When the amplitude ratio a is small, the AoLP and the DoLP are almost the same as those for the PG method (black dotted curve in the DoLP plots) as shown in Fig. 5(a) ($a = 0.2$). As a increases, the discrepancy in both the AoLP and the DoLP compared with those in the PG becomes more marked due to the contribution of the second-order harmonic shown in the comparison in Figs. 5(a)–5(c).

As clearly shown in Figs. 5(b)–5(d), the DoLP around $\text{AoLP} = 0^\circ$ has local maxima with a period of an integer multiple of the optical cycle of the fundamental pulse. When $\sin \omega T_d = 0$ or $T_d = nT_0$ ($n = 1, 2, 3, \dots$) in Eq. (16), $\text{AoLP} = 0^\circ$ where the emission polarization of the IAP is in

the x direction. In the following, we denote DoLP_θ as the DoLP at $\text{AoLP} = \theta$. DoLP_0 can be expressed as

$$\text{DoLP}_0 = D_0 \frac{1 + \frac{a^2 b}{4D_0}}{1 + \frac{a^2 b}{4}}. \quad (19)$$

Because D_0 is smaller than one, DoLP_0 is always larger than D_0 . In other words, the second-order harmonic contributes to increasing DoLP_0 .

On the other hand, when $\sin^2(\omega T_d/2) = 1$ or $T_d = (n + 1/2)T_0$ ($n = 1, 2, 3, \dots$) in Eq. (16), $\text{AoLP} = 90^\circ$ where the emission polarization of the IAP is in the y direction (perpendicular to the polarization direction of the second-order harmonic), and DoLP_{90} can be expressed as

$$\text{DoLP}_{90} = D_0 \frac{\left|1 - \frac{a^2 b}{4D_0}\right|}{1 + \frac{a^2 b}{4}}. \quad (20)$$

In this case, DoLP_{90} is smaller than D_0 , suggesting that the delay with $\text{AoLP} = 90^\circ$ is not efficient for generating the IAP because of the low intensity in the gating time window. The second-order harmonic contributes to suppressing the intensity in the gating time window when $\text{AoLP} = 90^\circ$.

The effect of the pulse duration ratio b on the DoLP and the AoLP is shown in the comparison between Figs. 5(b) and 5(d). When b is 2.0, where the pulse duration of the second-order harmonic is twice that of the fundamental pulse, the modulation of the DoLP is larger than when b is 1.0. In other words, DoLP_0 in DOG is larger than that in PG. At the same time, the variation of the AoLP decreases as T_d increases, suggesting that the polarization direction of the IAP is greatly affected by the polarization angle of the second-order harmonic, and there is no delay that gives $\text{AoLP} = 90^\circ$ where the IAP is generated perpendicular to the polarization direction of the second-order harmonic.

C. Robustness of the characterization methods

Here we discuss the robustness of the proposed characterization methods. The polarization filter array in the imaging polarimeter is composed of pixel-size linear polarizers oriented at four different angles ($0^\circ, 45^\circ, 90^\circ, 135^\circ$) as shown in Fig. 1(a). The intensity and polarization of the light should be uniform over a unit pixel for the polarization analysis defined by 2×2 pixels. In other words, when the intensity or the polarization of light changes sharply within a unit pixel for the polarization analysis, the retrieved DoLP and AoLP based on Eqs. (1) and (2) will exhibit a large error. When the laser beam is recorded with the imaging polarimeter, spatially uniform illumination in a unit pixel can be realized except for imaging of the focused beam. For example, the pixel size of the CMOS sensor (IMX250MZR, Sony) is $3.45 \mu\text{m}$ (and the unit pixel for the polarization analysis is $6.9 \mu\text{m}$) and is sufficiently small that it can be assumed that the parameters of the laser beam, such as intensity, spectrum, pulse duration, and polarization, are spatially uniform in the unit pixel.

Because both the DoLP and the AoLP are evaluated from a single-shot image, the precision of these parameters is determined by the signal-to-noise ratio in the CMOS sensor. The exposure time of the CMOS sensor should be set as short

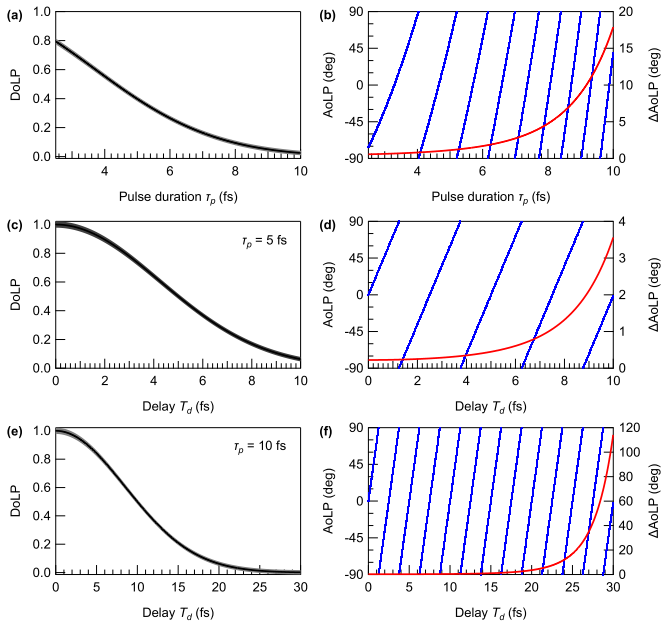


FIG. 6. (a) Pulse duration τ_p dependence of the DoLP (black) and associated errors (shaded area) where T_d is set to satisfy the gating condition $\tau_g = T_0/2$. (b) τ_p dependence of the AoLP (blue) and associated errors ΔAoLP (red). (c) and (d) Delay T_d dependence of the DoLP and the AoLP with their associated errors at $\tau_p = 5$ fs. (e) and (f) Delay T_d dependence of the DoLP and the AoLP with their associated errors at $\tau_p = 10$ fs.

as possible to minimize the dark current noise, and the readout noise is at least 3 orders of magnitude smaller than the full well capacity. Therefore, the contributions of the dark current and the readout noises are negligibly small for evaluating the DoLP and the AoLP.

A major source of errors in the DoLP and AoLP evaluations is fabrication flaws in the wire-grid polarizer array originating from variations in the wire thickness, the wire width, and the wire pitch, which affect the accuracy of the DoLP and the AoLP. However, the specification of the wire-grid polarizer array can be calibrated in advance to correct the quantum efficiency, the amplification gain, and the angle of polarizer for each pixel [29,30]. It is reported that calibrating the imaging polarimeter can reduce the error by 1 order of magnitude from 10% to 0.5% (DoLP) and 5.6% to 0.5% (AoLP) at the maximum illumination [29]. Because the imaging polarimeter [23], in which the wire-grid polarizers are placed in the vicinity of the photodiode, has a crosstalk smaller than that of conventional imaging polarimeters, a high accuracy for the DoLP and the AoLP is expected. Employing a binning operation for the image sensor and/or multiple image acquisition can further improve the signal-to-noise for determining the DoLP and the AoLP.

Another major source of error is shot noise which always exists in the CMOS sensor. In the following, we discuss the robustness of the characterization methods considering the shot noise as a primary source of errors.

1. Pulse duration τ_p dependence

In Figs. 6(a) and 6(b), the DoLP and the AoLP at $\tau_g = T_0/2$ and the associated errors calculated considering the shot noise are plotted as a function of the pulse duration τ_p of a Gaussian pulse with a central wavelength of 750 nm, where the maximum digital number of the CMOS sensor is set to 4095 counts considering the dynamic range (12 bits) of the imaging polarimeter. As τ_p increases, the DoLP decreases but the DoLP error does not depend on τ_p and is approximately 0.02 as shown in Fig. 6(a) because the Stokes parameter S_0 used in the evaluation of the DoLP does not depend on τ_p .

On the other hand, the AoLP error, ΔAoLP , depends on τ_p because S_1 and S_2 used for evaluating the AoLP become smaller as the DoLP becomes smaller. When $\tau_p = 5$ fs ($2T_0$) and 10 fs ($4T_0$), ΔAoLP are approximately 1.1° and 17.9° , respectively. These results suggest that the AoLP or the polarization direction can be determined with a precision better than 5° when the pulse duration τ_p of the driving laser pulse is shorter than 8.1 fs, corresponding to 3.2 optical cycles. When the dynamic range of the CMOS sensor is 16 bits, as in a scientific CMOS sensor, the AoLP and DoLP errors will be 1/4. Moreover, the errors in both the DoLP and the AoLP can be reduced by binning of the CMOS image sensor or the multiple frame image data acquisition by sacrificing the spatial resolution and the single-shot acquisition, respectively.

An advantage of the DOG method is that the duration of the driving laser pulse in DOG can be twice as long as that in PG [13]. Therefore, it is expected that ΔAoLP in DOG becomes larger when the duration of the driving laser pulse is set to twice that in PG. However, as shown in Fig. 5, the DoLP in DOG is larger than that in PG at $\text{AoLP} = 0^\circ$, and ΔAoLP in DOG will be smaller than that in PG when the duration of the fundamental laser pulse is identical.

2. Delay T_d dependence

In Figs. 6(c)–6(f), the DoLP and the AoLP at the fixed durations of the driving laser pulse ($\tau_p = 5$ and 10 fs) with a Gaussian pulse shape at a central wavelength of 750 nm and the associated errors calculated considering the shot noise are plotted as a function of the delay T_d . The error in the AoLP becomes larger as T_d increases, whereas the error in the DoLP is almost constant. When $\tau_p = 5$ fs, ΔAoLP is smaller than 4° at $T_d = 10$ fs corresponding to the second delay satisfying $\tau_g < T_0/2$ and $\text{AoLP} = 0^\circ$. On the other hand, when $\tau_p = 10$ fs, ΔAoLP is 17.2° at $T_d = 25$ fs, corresponding to the first delay satisfying $\tau_g < T_0/2$ and $\text{AoLP} = 0^\circ$.

These results suggest that the DoLP can be determined with an error of 0.02 irrespective of the pulse duration τ_p and the delay T_d , whereas the precision of the AoLP depends on τ_p and T_d . To determine the AoLP with a smaller error, the pulse duration of the driving laser pulse τ_p should be as small as possible because the AoLP error depends on the magnitude of the DoLP.

IV. SUMMARY

In this work, we propose a simple method for characterizing the parameters of gating methods for generating an IAP using an imaging polarimeter based on the division of the

focal plane. In the PG and DOG methods, the gate width and polarization direction of the IAP can be characterized as a snapshot approximately every 10 μm , corresponding to the unit pixel size of the polarization analysis in the imaging polarimeter. The two parameters, the DoLP and the AoLP, obtained from the imaging polarimeter are good measures for the gate width and the polarization direction, respectively. In the TCG method, the relative delay between the fundamental pulse and the second-order harmonic can be retrieved by measuring the full-Stokes parameters.

Since the polarization direction can be characterized in a single-shot, it can offer robust pump-probe measurements using the IAPs. The frame rate of the data acquisition will be limited by the frame rate of the CMOS image sensor in the imaging polarimeter. If we reduce the field of view by setting a region of interest, a frame rate higher than 1 kHz can be realized. Moreover, pixelated polarizers on a quadrant photodiode [31] can be utilized for evaluating the gating parameters with a repetition rate of more than 100 kHz.

Because the cutoff energy of high-order harmonics is proportional to λ^2 , driving laser pulses with longer wavelengths have been utilized to generate the IAPs using PG [32] and

DOG [33]. In particular, the idler pulse generated with optical parametric amplification is convenient for generating the IAP because the CEP is passively stabilized. Currently, the spectral range of a standard imaging polarimeter is limited by the spectral response of Si-CMOS. Broadband image sensors based on quantum dots and graphene (300–2000 nm) [34] will become available as alternatives to Si-CMOS for detecting light in the infrared wavelength region. In addition, full-Stokes imaging polarimeters in which the Stokes parameter for the circularity of the light can also be measured are currently being developed using dielectric metasurface masks [35,36] instead of the wire-grid polarizer array and will be able to characterize the gating parameters used in the PG and DOG methods.

ACKNOWLEDGMENTS

T.O. acknowledges financial support from JSPS Grants-in-Aid for Scientific Research (Grants No. JP15H03581 and No. JP20H02660) and JST PRESTO Grant No. JP-MJPR15P6, Japan. K.M. acknowledges financial support from JSPS Grants-in-Aid for Scientific Research (Grant No. JP19H05628).

-
- [1] F. Krausz and M. Ivanov, *Rev. Mod. Phys.* **81**, 163 (2009).
- [2] M. Nisoli, P. Decleva, F. Calegari, A. Palacios, and F. Martín, *Chem. Rev.* **117**, 10760 (2017).
- [3] M. F. Ciappina, J. A. Pérez-Hernández, A. S. Landsman, W. A. Okell, S. Zherebtsov, B. Förg, J. Schötz, L. Seiffert, T. Fennel, T. Shaaran *et al.*, *Rep. Prog. Phys.* **80**, 054401 (2017).
- [4] P. B. Corkum, *Phys. Rev. Lett.* **71**, 1994 (1993).
- [5] G. Sansone, L. Poletto, and M. Nisoli, *Nat. Photonics* **5**, 655 (2011).
- [6] M. Chini, K. Zhao, and Z. Chang, *Nat. Photonics* **8**, 178 (2014).
- [7] I. Orfanos, I. Makos, I. Lontos, E. Skantzakis, B. Förg, D. Charalambidis, and P. Tzallas, *APL Photonics* **4**, 080901 (2019).
- [8] P. B. Corkum, N. H. Burnett, and M. Y. Ivanov, *Opt. Lett.* **19**, 1870 (1994).
- [9] O. Tcherbakoff, E. Mével, D. Descamps, J. Plumridge, and E. Constant, *Phys. Rev. A* **68**, 043804 (2003).
- [10] G. Sansone, E. Benedetti, F. Calegari, C. Vozzi, L. Avaldi, R. Flammini, L. Poletto, P. Villoresi, C. Altucci, R. Velotta, S. Stagira, S. De Silvestri, and M. Nisoli, *Science* **314**, 443 (2006).
- [11] I. J. Sola, E. Mével, L. Elouga, E. Constant, V. Strelkov, L. Poletto, P. Villoresi, E. Benedetti, J.-P. Caumes, S. Stagira, C. Vozzi, G. Sansone, and M. Nisoli, *Nat. Phys.* **2**, 319 (2006).
- [12] Y. Oishi, M. Kaku, A. Suda, F. Kannari, and K. Midorikawa, *Opt. Express* **14**, 7230 (2006).
- [13] Z. Chang, *Phys. Rev. A* **76**, 051403(R) (2007).
- [14] C. Marceau, G. Gingras, and B. Witzel, *Opt. Express* **19**, 3576 (2011).
- [15] A. T. J. B. Eppink and D. H. Parker, *Rev. Sci. Instrum.* **68**, 3477 (1997).
- [16] H. Wang, M. Chini, S. Chen, C.-H. Zhang, F. He, Y. Cheng, Y. Wu, U. Thumm, and Z. Chang, *Phys. Rev. Lett.* **105**, 143002 (2010).
- [17] M. Reduzzi, W.-C. Chu, C. Feng, A. Dubrouil, J. Hummert, F. Calegari, F. Frassetto, L. Poletto, O. Kornilov, M. Nisoli, C.-D. Lin, and G. Sansone, *J. Phys. B: At., Mol. Opt. Phys.* **49**, 065102 (2016).
- [18] M. Nisoli, S. De Silvestri, O. Svelto, R. Szipöcs, K. Ferencz, C. Spielmann, S. Sartania, and F. Krausz, *Opt. Lett.* **22**, 522 (1997).
- [19] C. Hauri, W. Kornelis, F. Helbing, A. Heinrich, A. Couairon, A. Mysyrowicz, J. Biegert, and U. Keller, *Appl. Phys. B* **79**, 673 (2004).
- [20] C.-H. Lu, Y.-J. Tsou, H.-Y. Chen, B.-H. Chen, Y.-C. Cheng, S.-D. Yang, M.-C. Chen, C.-C. Hsu, and A. H. Kung, *Optica* **1**, 400 (2014).
- [21] C.-H. Lu, T. Witting, A. Husakou, M. J. Vrakking, A. H. Kung, and F. J. Furch, *Opt. Express* **26**, 8941 (2018).
- [22] J. E. Beetar, S. Gholam-Mirzaei, and M. Chini, *Appl. Phys. Lett.* **112**, 051102 (2018).
- [23] Y. Maruyama, T. Terada, T. Yamazaki, Y. Uesaka, M. Nakamura, Y. Matoba, K. Komori, Y. Ohba, S. Arakawa, Y. Hirasawa, Y. Kondo, J. Murayama, K. Akiyama, Y. Oike, S. Sato, and T. Ezaki, *IEEE Trans. Electron Devices* **65**, 2544 (2018).
- [24] M. Möller, Y. Cheng, S. D. Khan, B. Zhao, K. Zhao, M. Chini, G. G. Paulus, and Z. Chang, *Phys. Rev. A* **86**, 011401(R) (2012).
- [25] T. Mu, D. Bao, F. Han, Y. Sun, Z. Chen, Q. Tang, and C. Zhang, *Opt. Express* **27**, 23009 (2019).
- [26] H. Mashiko, S. Gilbertson, C. Li, S. D. Khan, M. M. Shakya, E. Moon, and Z. Chang, *Phys. Rev. Lett.* **100**, 103906 (2008).
- [27] S. Gilbertson, H. Mashiko, C. Li, S. D. Khan, M. M. Shakya, E. Moon, and Z. Chang, *Appl. Phys. Lett.* **92**, 071109 (2008).
- [28] G. Ghosh, *Opt. Commun.* **163**, 95 (1999).
- [29] S. B. Powell and V. Gruev, *Opt. Express* **21**, 21039 (2013).

- [30] J. Zhang, H. Luo, B. Hui, and Z. Chang, *Appl. Opt.* **55**, 7236 (2016).
- [31] C. He, J. Chang, Y. Wang, R. Liao, H. He, N. Zeng, and H. Ma, *Appl. Opt.* **54**, 4458 (2015).
- [32] J. Li, X. Ren, Y. Yin, Y. Cheng, E. Cunningham, Y. Wu, and Z. Chang, *Appl. Phys. Lett.* **108**, 231102 (2016).
- [33] J. Li, A. Chew, S. Hu, J. White, X. Ren, S. Han, Y. Yin, Y. Wang, Y. Wu, and Z. Chang, *Opt. Express* **27**, 30280 (2019).
- [34] S. Goossens, G. Navickaite, C. Monasterio, S. Gupta, J. J. Piqueras, R. Pérez, G. Burwell, I. Nikitskiy, T. Lasanta, T. Galán, E. Puma, A. Centeno, A. Pesquera, A. Zurutuza, G. Konstantatos, and F. Koppens, *Nat. Photonics* **11**, 366 (2017).
- [35] E. Arbabi, S. M. Kamali, A. Arbabi, and A. Faraon, *ACS Photonics* **5**, 3132 (2018).
- [36] N. A. Rubin, G. D'Aversa, P. Chevalier, Z. Shi, W. T. Chen, and F. Capasso, *Science* **365**, eaax1839 (2019).